

1 Possible Titles

The effect of roughness on the elasticity and permeability of fractured media

The relation between changes in permeability and elastic wave velocity in dynamically stressed fractured rocks

The relation between transient changes in permeability and elastic wave velocity in dynamically stressed fractured rocks

Elastodynamic and poromechanical properties of fractured rock

Characterizing the elastodynamic and poromechanical properties of fractured rock with dynamic stressing

An experimental investigation of the coupling between elastodynamic and hydraulic properties of naturally fractured rock at the laboratory scale

Elastodynamic and hydraulic properties of fractured and sheared rock: An experimental investigation

2 Abstract

We describe laboratory work to elucidate the relationship between nonlinear elasticity and permeability of fractured media subjected to local stress perturbations in relation to fracture roughness and aperture distribution. This study is part of an effort to image fluid pathways and fracture properties using locally induced seismicity, associated with fluid injection. Experiments were conducted in which intact L-shaped Westerly Granite samples were fractured in-situ tri-axial conditions while forcing deionized water through the subsequent fracture interfaces. After in-situ fracture, we imposed oscillations of the applied Normal stress and pore pressure with amplitudes ranging from 0.2 to 1 MPa and frequencies from 0.1 to 10 Hz. During these dynamic perturbations an array of ultrasonic transducers (PZTs) continuously generated and transmitted p-wave pulses to monitor the elastic response of the granite samples. We interpret the relative change in p-wave velocities to be an analog for the elastic non-linearity and relate it to the permeability of the fractured media. The roughness of the fracture interfaces is altered during experiments by shearing the L-shaped samples and then allowing the interface to age before applying dynamic stressing. We observe changes in the permeability and stiffness of the fracture during the dynamic perturbations and also with the shearing history, changing roughness, of the Westerly Granite samples.

3 Introduction

Dynamic stresses associated with energy production and waste water sequestration (injection, pumping, and transport of supercritical H_2O-CO_2 fluids) are particularly concerning as they are known to induce seismicity [Healy et al., 1968; Raleigh et al., 1976; Simpson et al., 1988; Sminchak and Gupta, 2003; McNamara et al., 2015; McGarr et al., 2015; Walsh and Zoback, 2015].

Though dynamic stressing could be beneficial for enhanced permeability, it presents a significant risk associated with fault reactivation, reservoir seal damage, and accelerated deformation. Therefore, it is important to understand how fluid injection influences the hydromechanical properties of rocks and fractures. We have performed careful laboratory experiments to investigate the connection between fluid flow and elastic nonlinearity (i.e. stress is not proportional to strain) of fractured media.

Dynamic stressing of the local subsurface associated with seismicity, drilling, hydraulic injection cause transient changes in permeability. These perturbations cause significant changes in the local stress field and consequently the poromechanical properties of the local subsurface. Empirical evidence from the field and laboratory show that earthquakes and subsequent seismic waves cause transient changes in rock stiffness in the proximity of faults. Specifically, measurements of a sudden decrease in seismic wave velocity from co-seismic softening and a post-seismic relaxation of the rock stiffness, a logarithmic recovery in time. Scaling down to laboratory studies, it has been shown that by using dynamic acousto-elastic testing, ultrasonic wave velocity (analog for field-scale seismometers) recorded decreased during dynamic stressing and then recovered after dynamic stressing ended with a logarithmic form. Dynamic perturbations with strain on the order of 10^{-6} cause a transient decrease in stiffness in nonlinear elastic materials.

Anthropogenic activities on the field-scale such as drilling, wastewater storage, hydraulic fracturing result in considerable deformation of reservoir rocks. Changing the hydromechanical properties by dynamic stressing from fluid injection are likely to present hazards in the form of fault reactivation and reservoir seal damage. Evidence of this type of stressing inducing regional seismicity is rich and numerous (*more details and citations*). Despite the hazards, dynamic stressing of the subsurface may result in enhanced permeability, consequently greater energy recovery. Seismic and anthropogenic sources of dynamic perturbation both change rock stiffness and permeability in similar ways, which suggests there is a physical mechanism that relates the nonlinear stiffness and poromechanical properties of fractured rock.

Nonlinear response is sensitive to many fracture properties: geometry, flow pathways, asperity compliance, and friction. Currently, literature for investigating the relationship b/w elastodynamic and poromechanical and subsequent recovery is quite limited. We present the results from sophisticated well-controlled laboratory experiments in which we combine the analysis of nonlinear elastodynamic and hydraulic data.

It is expected that the nonlinear behavior of rocks is sensitive to fine features such as fracture aperture (i.e. flow pathways, asperity stiffness). In order to fully understand the ramifications of dynamic stressing in the subsurface, we need elucidate the relationship between the elastodynamic and hydro-mechanical properties of fractured rocks.

4 Experimental Setup

We conducted sophisticated experiments in which samples were loaded under triaxial conditions inside a pressure vessel and fractured in-situ to simultaneous measure flow rate and elastic properties. Westerly granite samples were prepared by cutting them into L-shape blocks (69 x 45 50 x 26 mm, Figure 1) with 3 mm deep notches on the top and bottom to ensure reproducibility of planar fracture propagation. The L-shape is used for maintaining constant nominal contact area during fracture and shear. The samples were saturated in deionized water and then placed between steel forcing blocks that have embedded piezoelectric transducers. The P-polarized lead-zirconate transducers (PZTs) of company APC International Ltd. are 6.5 mm in diameter, with a center frequency of 500 kHz and the spacing between the steel loading platen and the PZTs is 4mm. The shorter forcing block additionally contains internal conduits to provide fluid flow along the fracture plane. Deionized water was pumped through these narrow channels (45 x 1 mm) and covered by sintered porous fits and fed by five 1.6 mm diameter holes. Sintered porous frits (permeability $10^{-14} m^2$) are press-fit into cavities within the short forcing block to allow homogenous distribution of fluid. After securing this Single Direct Shear (SDS) configuration, it was sealed inside a latex jacket to separate confining and pore fluids. Fully prepared and jacketed samples were fitted inside a pressure vessel within a biaxial loading apparatus.

The Biax consists of two hydraulic pistons capable of applying vertical and horizontal loads in displacement or load control. Forces are measured using custom-built, beryllium-copper strain-gauge load cells mounted on each loading piston. The load cells have an amplified output of ± 5 V with an accuracy of ± 5 N and are calibrated with a Morehouse proving-ring. Displacements are measured with direct-current displacement transducers (DCDT), with an accuracy of $\pm 0.1 \mu\text{m}$. The confining fluid, a food-grade heat transfer oil (XCELTERM 600, Radco Industries), in the sealed pressure vessel is pressurized to create a true-triaxial stress conditions. A linear variable differential transformer was attached to the outside of the sample, inside the pressure vessel, to accurately ($\pm 0.1 \mu\text{m}$) measure the fracture displacement. Pressure intensifiers fitted with LVDTs and pressure transducers were used to control the confining pressure and the internal upstream and downstream pressures.

Each axis of loading is independently servo-controlled and all stresses, strains, fluid pressures and fluid volumes were recorded with ± 10 V, 16-channel 24-bit analog-to-digital converter at 10 kHz and averaged to sampling rates of 100 Hz or 1 kHz. Fracture permeability was measured using upstream and downstream pore-pressure intensifiers. Active ultrasonic data were recorded using a VantageTM Research Ultrasound (Verasonics) system. We use broadband (0.02-2 MHz) PZTs (APC International Ltd. 6.35 diameter compressional crystals), which were successively pulsed every 1 ms on the transmitting side and the recording rate at the receiver side was 25 MHz. The input signal is a half sine with a frequency of 500 kHz. Also, a pulse from the Verasonics system accompanied the PZT excitation and is recorded by the 24-bit analog-to-digital data acquisition system. This allows us to sync the “ultrasonic” to “poro-mechanical” data and then analyzed to measure changes in the permeability and elasticity of the fractured rock samples, explained more fully in the signal analysis procedure.

Before commencing each experiment, the samples were installed in the pressure vessel and then the vessel was sealed and then filled with confining fluid. A horizontal load of 20 MPa was applied and then the confining fluid pressure was slowly increased to 15 MPa; it is important to monitor the integrity sample jacket seal during this step. Next, we applied a pore pressure differential: inlet ($P_{pA} = 4$ MPa) and outlet ($P_{pB} = 2$ MPa). At this point there was no flow because Westerly granite matrix permeability is very low ($< 10^{-20} \text{ m}^2$) and the confining fluid pressure is greater than the pore pressure (there was no flow around the sample). After establishing all loads and pore pressure, the ultrasonic data acquisition Once all fluid pressures and solid stresses were applied, the ultrasonic data acquisition system (Verasonics[®]) was started. The sample was then fractured in situ by increasing the shear stress at constant normal stress while making continuous measurements of fluid flow and ultrasonic properties. After locking the vertical piston (no displacement allowed), we executed the dynamic stressing protocol illustrated in Figure 2a.

After executing the normal stress and pore pressure oscillation protocol, the fractured sample was sheared twice in 4 mm increments (for a total of 8 mm). During the shearing phases of the experiment acoustic emissions (AEs) were monitored (passive source recording). Subsequent to shearing the dynamic stressing protocol was repeated. We incorporate shearing in this investigation to determine its influence on the non-linearity measurements of the fracture. The fracture aperture is changed through shear, in effect, modeling the complexity of fractured subsurface rock.

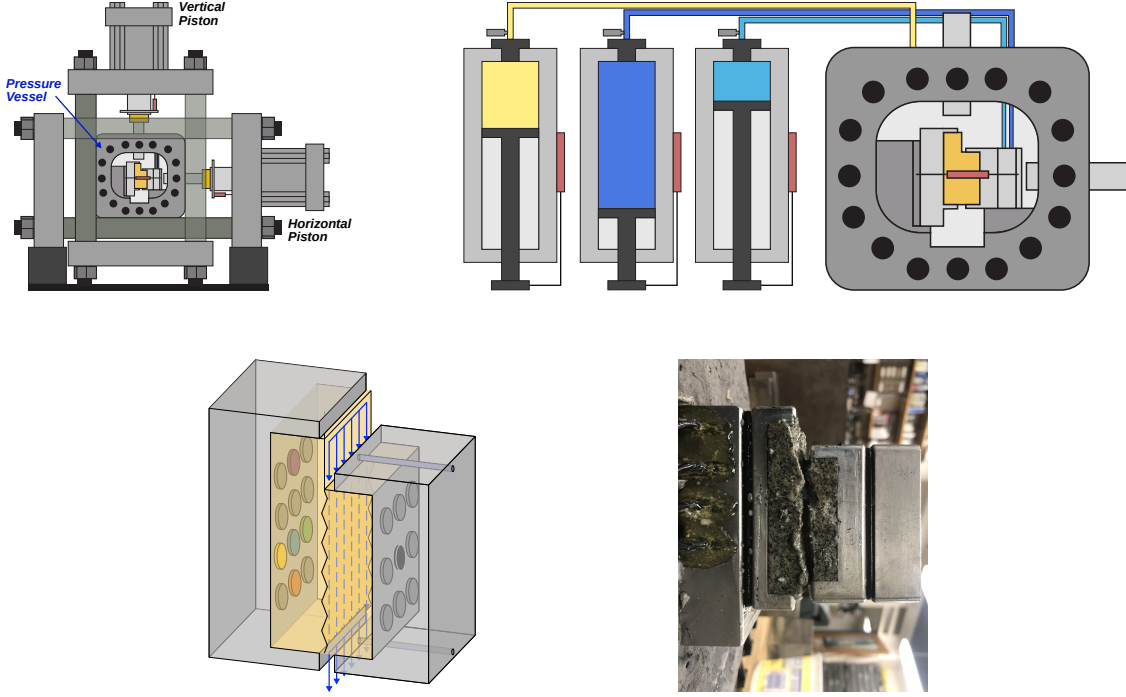


Figure 1: (a) The experiments were conducted in the Penn State Rock and Sediment Mechanics laboratory using the Biaxial Deformation Apparatus (Biax). The Biax has servo-controlled vertical and horizontal pistons and a 10 kHz 24-bit analog to digital data recorder. (b) A pressure vessel was inserted in the Biax and connected to the pressure intensifiers, which control the confining (P_C), and sample (P_{PA} and P_{PB}) fluid pressures. (c) The Westerly granite sample is machine cut into a L-shape and placed between the two loading platens. These loading platens are embedded with piezoelectric transducers (p-polarized) and contain fluid ports for the inlet and outlet flow. The shorter forcing block additionally contains internal conduits to provide fluid flow along the fracture plane. Deionized water was pumped through these narrow channels (45×1 mm) and covered by sintered porous fits and fed by five 1.6 mm diameter holes. Sintered porous frits (permeability $\sim 10^{-14} \text{ m}^2$) are press-fit into cavities within the short forcing block to allow homogeneous distribution of fluid. After securing this Single Direct Shear (SDS) configuration, it was sealed inside a latex jacket to separate confining and pore fluids. (d) A photo of the sample after experimentation highlights the degree of roughness of the in-situ fracture.

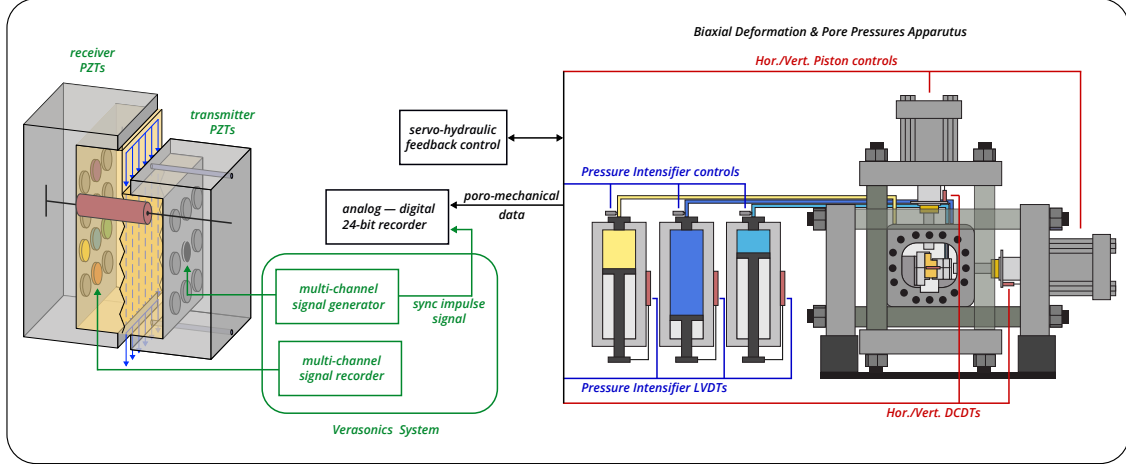


Figure 2: Schematic of the single direct shear configuration with the block diagram showing the main features of the data acquisition system for both the poro-mechanical and ultrasonic data. The Biax consists of two hydraulic pistons capable of applying vertical and horizontal loads in displacement or load control. Forces are measured using custom-built, beryllium-copper strain-gauge load cells mounted on each loading piston. The load cells have an amplified output of 5 V with an accuracy of 5 N and are calibrated with a Morehouse proving-ring. Displacements are measured with direct-current displacement transducers (DCDT), with an accuracy of $\pm 0.1\mu\text{m}$. Each axis of loading is independently servo-controlled and all stresses, strains, fluid pressures and fluid volumes were recorded with 10 V, 16-channel 24-bit analog-to-digital converter at 10 kHz and averaged to sampling rates of 100 Hz or 1 kHz. Fracture permeability was measured using upstream and downstream pore-pressure intensifiers. Active ultrasonic data were recorded using a Vantage TM Research Ultrasound (Verasonics) system. We use broadband (0.02-2 MHz) PZTs (APC International Ltd. 6.35 mm diameter compressional crystals), which were successively pulsed every 1 ms on the transmitting side and the recording rate at the receiver side was 25 MHz. The input signal is a half sine with a frequency of 500 kHz. Also, a pulse from the Verasonics system accompanied the PZT excitation and is recorded by the 24-bit analog-to-digital data acquisition system. This allows us to sync the ultrasonic to poro-mechanical data and then analyzed to measure changes in the permeability and elasticity of the fractured rock samples, explained more fully in the signal analysis procedure.

4.1 Dynamic Effective Stress Perturbations

The fractured samples were dynamically perturbed via pore pressure (P_P) and normal stress (σ_n) oscillations. Following the procedure described by Candela et al., 2015, pore pressure oscillations were achieved by oscillating P_{PA} while holding P_{PB} constant. Conversely, normal stress oscillations were applied by oscillating the horizontal piston of the load frame at prescribed amplitude and frequency. As depicted in Figure 2a, multiple sets of P_P and σ_n oscillations of varying amplitude (up to about \pm MPa) and frequency (0.1, 1, 10 and 40 Hz) were applied to investigate the repeatability as well as amplitude and frequency dependencies of the measured response. Similar parameters were used for P_P and σ_n oscillation sets in order to apply similar effective stress perturbations and allow making comparisons between P_P and σ_n stimulations.

4.2 Permeability Measurements

We measured flow rates independently at the inlet (Q_A) and outlet (Q_B) using the outputs of LVDTs on the pressure intensifiers. After verifying the steady state flow condition ($Q_A - Q_B \leq 5\%$), Darcy's law was used to calculate permeability k :

$$k = \frac{\mu L}{S} \frac{Q}{\Delta P_P} \quad (1)$$

where $Q = \frac{1}{2}(Q_A + Q_B)$ is the average flow rate ($\frac{m^3}{s}$), μ is the fluid viscosity ($10^{-3} Pa \cdot s$) at $20^\circ C$, L is the flow path given by the length of the sample (50 mm) and S is the cross section perpendicular to the flow path (45 x 26 mm^2).

Specifically, k is the bulk permeability, that is, the permeability of the surrounding rock matrix (on order of $10^{-21} m^2$) and of the fracture [Zhang et al., 2017; Ishibashi et al., 2018]. Alternative calculations of permeability are valid [Zhang et al., 2017; Ishibashi et al., 2018], however we are interested in relative changes in permeability in response to dynamic stressing, so the absolute value of the permeability is not necessary to quantify.

4.3 Ultrasonic Measurements: Active Source

Ultrasonic waves transmitted through the fracture were recorded continuously in each experiment. Half-cycle sinusoidal pulses with an amplitude of 40 V and center frequency of 500 kHz were emitted consecutively from each transmitting transducer (9 piezoelectric discs arranged in a 3 x 3 matrix embedded within the right-hand loading block in Figure 1b) with a pulse repetition frequency (PRF) of 100 Hz or 1000 Hz during the low and high frequency (≥ 10 Hz) stress oscillations, respectively. The waveforms were amplified (~ 40 dB) and recorded for all the receiving transducers (12 piezoelectric discs arranged in a 4 x 3 matrix embedded within the left-hand loading block in Figure 1b). We activated up to the full array of 9 transmitter and 12 receivers.

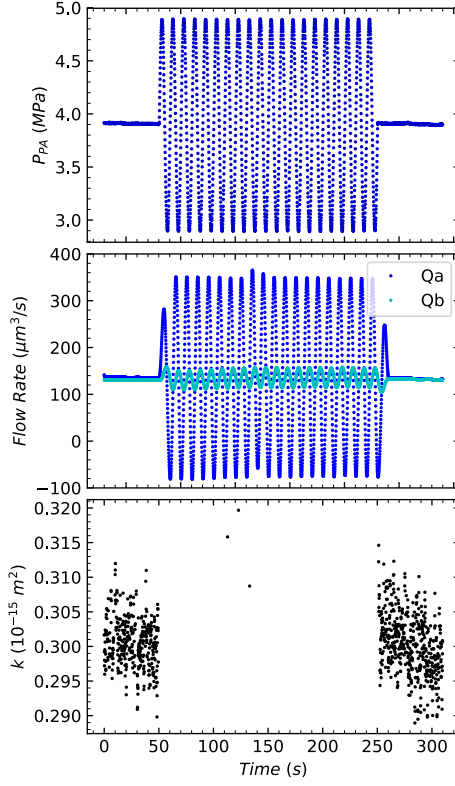


Figure 3: Example of dynamic stressing and the corresponding flow rate measurements for a set of pore pressure oscillations in experiment p4975. Note that the plots (a) and (b) are decimated for clarity. (a) Imposed pore pressure oscillation at inlet and fixed pore pressure at the outlet. Pressure conditions before and after the oscillations are identical. (b) Measured flow rates at the fracture inlet (blue line) and outlet (red dashed line). Notice the small time lag (≤ 2 s) between the maxima of the inlet and outlet flow rates. (c) Permeability at steady-state and during the pore pressure oscillation. In the calculation of permeability we impose a threshold between the flow rates to ensure steady-state flow ($Q_A - Q_B \leq 5\%$). It is reasonable to assume that even at relatively low frequency oscillations, there is effectively no steady-state flow during the imposed oscillations.

We measure the effective permeability, k_a , by calculating the flow rate over a 2 s window. For pore pressure oscillations, we start 10 s after the oscillation to ensure that permeability measurement is not affected by the P_p oscillation and/or by storage effects. Need to annotate Flow Rate with lines indicating the $\pm 5\%$

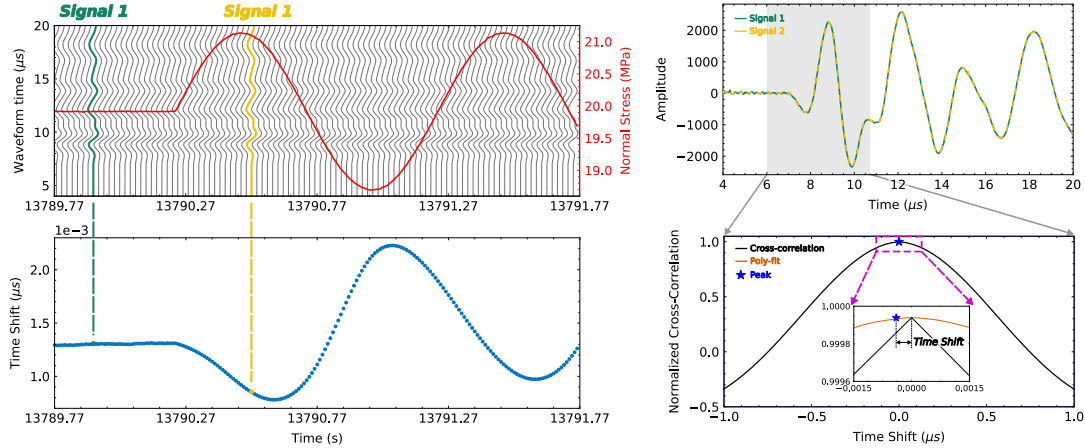


Figure 4: (a) Excerpt from run4 of experiment p4966 shows part of a 1 Hz, 1 MPa normal stress oscillation (red) and the concurrent raw ultrasonic waveforms (grey). The number of waveforms in the waterfall plot has been decimated version for clarity. (b) Time shift was calculated by cross-correlating the waveforms to a reference waveform. (c) An example of a reference, unperturbed, waveform (green) and perturbed waveform (dashed yellow) highlights the similarity. (d) The maximum linear correlation between the reference and perturbed waveforms from cross-correlation is used to determine the time shift. The inset shows improvement of time shift calculations with a 2nd order polynomial fitting procedure.

5 Experimental Procedure

Each experiment commenced with extensive sample preparation: in which the Westerly granite was cut and notched, sealed in a latex jacket, and then placed inside the pressure vessel (see Section 4 for details). After sealing the pressure vessel and loading the sample, inlet and outlet flow were pressurized to 4 MPa and 2MPa, respectively. At this stage there was no flow because Westerly granite matrix permeability is very low ($< 10^{-20} \text{ m}^2$) and the confining fluid pressure (around the jacketed sample) is much larger than the pore pressure, preventing flow of water around the sample. A shear load was then applied with the vertical piston in displacement mode at a constant $10 \mu\text{m/s}$, fracturing in-situ after reaching a critical stress of $\approx 60 \text{ MPa}$, and then locked the vertical piston. During fracture fluid flow and acoustic emissions were measured, but these results are not included in this paper. Next, the dynamic stressing protocol was implemented in which the normal stress and pore pressure were modulated. Normal stress oscillations were applied by oscillating the horizontal piston of the load frame at prescribed amplitudes (0.2 to 3 MPa) and frequencies (0.1, 1, 10, 40 Hz). Pore pressure oscillations were achieved by oscillating P_{PA} while holding P_{PB} constant at amplitudes of 0.2 to 3 MPa and frequencies of 0.1, 1, 10 Hz. Multiple sets of normal stress and pore pressure oscillations of varying amplitudes and frequencies were applied to investigate: (1) repeatability and direct comparison between the two modulated stresses and (2) amplitude and frequency dependencies of the measured response. Post-fracture dynamic stressing is plotted in Figure 5d (highlighted in yellow) and shows the normal stress (red) and pore pressure (blue) oscillations; note that line thickness correlates with oscillation frequency. To investigate the effect of fracture aperture on elastic nonlinearity and permeability, the sample was sheared in two 4 mm, (held at $\sigma_{NS} = 20 \text{ MPa}$) stages. After each shearing stage the oscillation protocol was applied to the sample. Initially, the in-situ fracture was quite rough, but the effect of shear reduces and changes this roughness; the old contacts were broken and new contacts formed, changing the extent to which the two halves of the fracture were mated. This allows for investigation of how fracture aperture is related to the elasto-dynamic and hydromechanical properties.

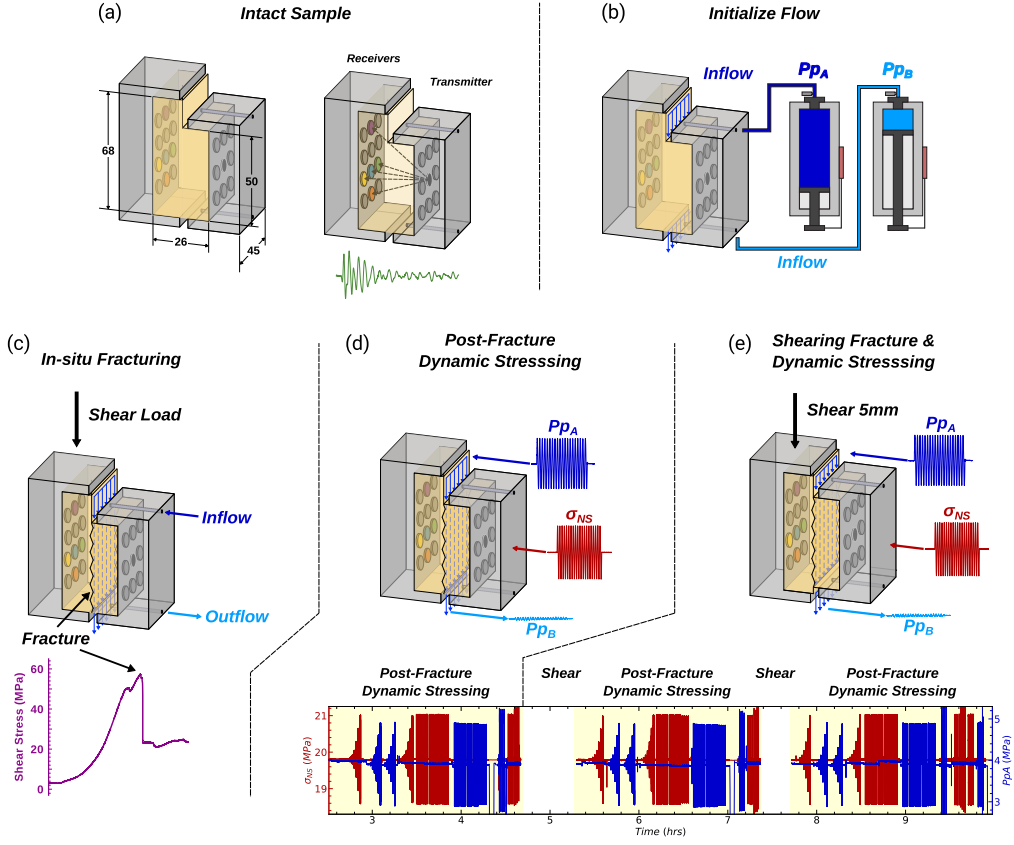


Figure 5: (a) Intact Westerly granite sample cartoon, showing dimensions and approximate transmitter - receiver ray paths. (b) Next, we applied a pore pressure differential: inlet ($P_{pA} = 4$ MPa) and outlet ($P_{pB} = 2$ MPa). (c) The shear stress was loaded at a constant rate of $10 \mu\text{m/s}$ until reaching the critical shear stress at ≈ 60 MPa. (d) Cartoon showing the oscillation protocol applied to the freshly fractured sample. Multiple sets of P_P and σ_{NS} oscillations of varying amplitude (up to about ± 1 MPa) and frequency (0.1, 1, 10 and 40 Hz) were applied. (e) The sample was sheared in two additional increments of 4mm, each followed by the dynamic stressing protocol.

In order to quantify the nonlinearity of the fractures, we first obtain the evolution of ultrasonic wave amplitude (Figure 2b) and velocity (Figure 2c) from the continuously measured ultrasonic data (Shokouhi et al., 2019) and calculate three parameters: (1) the average or DC-change in wave velocity due to the imposed oscillations, (2) the amplitude of steady-state velocity fluctuation during the oscillations, and (3) the recovery rate of wave velocity post oscillation (Figure 2c). The relative velocity change ($\Delta c/c_0$) is defined as the % change in velocity due to the imposed normal stress or pore pressure oscillation. We calculate $\Delta c/c_0$ from the velocity before (c_0) and after (c) each oscillation averaged over 1-s time windows as depicted in Figure 2c. At a given oscillation amplitude, the more negative the $\Delta c/c_0$ (larger absolute value), the more nonlinear is the fracture. The parameter dc/c_0 is defined as the amplitude of velocity oscillations, averaged over the oscillation duration and normalized by pre-oscillation velocity c_0 (Figure X). Similar to $\Delta c/c_0$, a larger magnitude of dc/c_0 at a given oscillation amplitude is an indication of higher nonlinearity. The third parameter \dot{c} is defined as the (logarithmic) rate of recovery of wave velocity after the oscillation is removed (Figure 2c). Materials of higher nonlinearity are expected to have slower recoveries (Shokouhi et al., 2017b). In the next section, we discuss the dependence of $\Delta c/c_0$, dc/c_0 , and \dot{c} (Figure X) on the imposed normal stress and pore pressure amplitudes as well as frequency. In addition, we compare the measured nonlinearities before and after shearing the fracture. This comparison provides insight into how changes in the aperture size distribution (due to shearing and wear) and the presence of fines alter the fracture stiffness and the stress-dependency of the elastodynamic response. Although not shown here, similar nonlinearity parameters may be extracted from the evolution of ultrasonic wave amplitude (Figure X).

6 Results

As previously specified, the ultrasonic waveforms are combined with strain measurements to calculate the nonlinear elastodynamic response and flow rates are used to determine fracture permeability. These measurements allow us to ascertain how the in-situ fracture responds to dynamic stressing. In other words, the imposed oscillations that range in amplitude and frequency probe the elastodynamic and hydraulic properties of the fractured samples.

6.1 Nonlinear elastodynamic and hydraulic responses

From Parisa's Arma: We measure the nonlinearity of the elastodynamic response directly by quantifying the stress-dependency of wave velocity and amplitude. Figure 6 depicts the typical response of our fractured samples to dynamic stress perturbations. Immediately after effective stress oscillations, the fractured rock exhibits an instantaneous softening i.e., the wave velocity c_0 suddenly drops. However, if the dynamic perturbation is not too strong, this softening is transient; once the oscillation is removed, the wave velocity oscillates in response to dynamic stress at frequencies that are harmonics of the excitation frequency. The average amplitude of these oscillations (at the oscillation frequency) is denoted as dc in Figure X. If the stress oscillations persist, the changes in wave velocity reach a non-equilibrium steady state. This characteristic response (transient softening, slow recovery and velocity fluctuations) is a signature of nonlinear mesoscopic elasticity (Guyer and Johnson, 2009) and rich in information on microstructure, fractures and contact mechanics. In comparison, the wave velocity in a linear elastic medium is stress-invariant i.e., $c = c_0$ before, during and after stress oscillations. Most intact rocks exhibit some degree of nonlinearity due to soft grain boundaries and microcracks in their matrix (Rivière et al., 2015). However, when fractured, their nonlinear electrodynamic responses are also influenced by the contact acoustic nonlinearity (CAN) at the rough fractured interface.

The recovery rate captures the late-time slow dynamic behavior of the three sample conditions. As previously described, following the dynamic perturbation, the wave velocity drops due to an instantaneous elastic softening as shown in Figure 4 (b). Once the oscillation is removed, the wave velocity slowly increases towards the pre-oscillation value (c_0). The 90-second hold time between successive oscillations is sufficient for most of the relaxation to take place, although a full recovery may take significantly longer (Renaud, Le Bas and Johnson, 2012). Regardless of the state, the wave velocity follows a time-logarithmic trend as illustrated in Figure 8 for a 1 MPa-oscillation at 10 Hz. This observation is consistent with previous observations (Ten Cate and Shankland, 1996; Shokouhi, Rivière, Guyer, et al., 2017; Shokouhi, Rivière, Lake, et al., 2017), where a late-time time-logarithmic recovery is reported.

In order to quantify the recovery rate, the late-time recovery of wave velocity is described by an equation of the form $c = p_1 \log t + p_2$, where p_1 and p_2 are the slope (recovery rate) and intercept respectively. Figure 9 shows the amplitude- and frequency-dependency of the slope p_1 . We observe that p_1 increases with the normal stress oscillation amplitude and decreases with the frequency of oscillations. Of the three-sample states, p_1 is the largest for the dry intact sample and smallest for the saturated fractured condition. This observation is consistent with that reported for the other two nonlinearity parameters discussed above.

The details on amplitude- and frequency-dependencies of $delc/c_0$ and dc/c_0 for a single transmitter-receiver pair are given in Shokouhi et al. (2019). Similar trends are observed for all transmitter-receiver pairs and therefore, not repeated here. In summary, the results given in Shokouhi et al. (2019) indicate that $delc/c_0$ and dc/c_0 are modulated by dynamic stress amplitudes for both pore pressure oscillations and fracture normal stress oscillations (Figure 3 and Figure 4). In addition, the measurements exhibit frequency-dependence (not shown here); $delc/c_0$ increases with the oscillation frequency, while dc/c_0 mostly decreases. Observing different trends for the different nonlinearity parameters is not surprising. Although the origins of $delc/c_0$ and dc/c_0 remain unclear, there is empirical evidence that they stem from different micro-mechanical mechanisms (Rivière et al., 2016, 2015). Although the c . values tend to generally increase with the oscillation amplitude, we do not observe a clear trend (not shown). This could be in part due to the variability in c . caused by the low signal-to-noise ratio. The recovery rate c . does not show a systematic dependency on frequency (not shown).

Shearing of the fracture reduces dc/c_0 during normal stress oscillations (Figure 4a). Interestingly, we have recorded different post-shear behavior for normal stress vs. pore pressure oscillations; the shearing increases the nonlinearity during pore pressure oscillations for one sample (p4975), while decreasing it for the other sample (p4966) (Figure 4b). This and other observations indicate possible differences in mechanisms activated during these two modes of dynamic stressing. On the other hand, shearing does not have a significant influence on $\Delta c/c_0$. The second shearing step decreases the measured nonlinearity $\Delta c/c_0$ but only slightly.

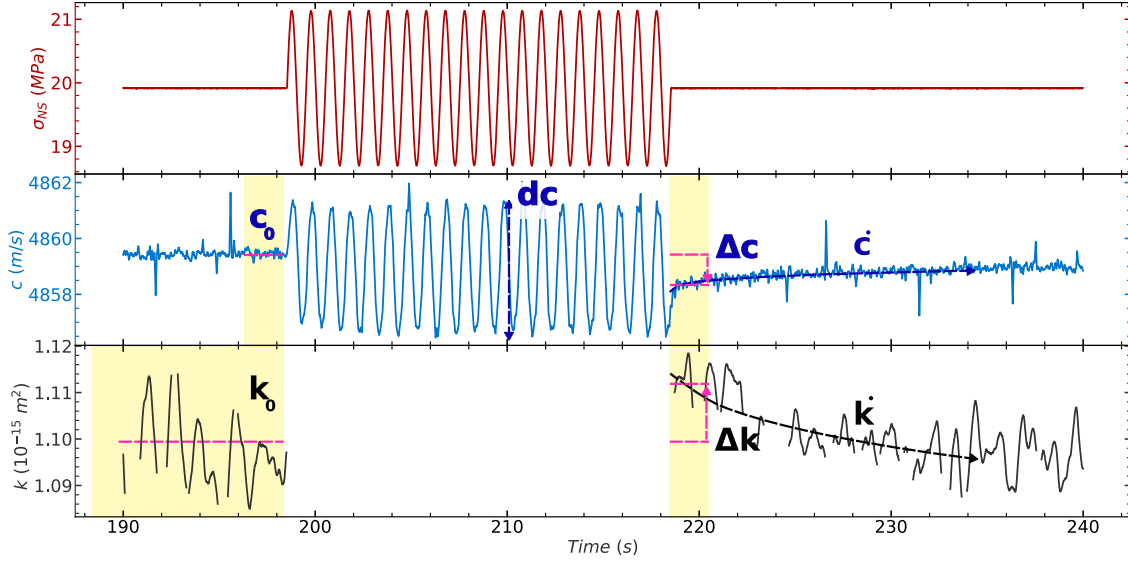


Figure 6: The velocity and permeability changes are calculated using the measured values before and after each oscillation averaged over the time windows (gray boxes) shown in (c). Data points in the permeability measurements are omitted on the condition that inlet/outlet flow rates differ $> 5\%$. That is to say, plotted permeability points represent when there is steady-state flow, necessary for Darcy's law. Dashed lines indicate the recovery of p-wave velocity (\dot{c}) and permeability (\dot{k}), respectively, from post-oscillation response to new steady-state value. Furthermore, we parameterize the p-wave velocity change dc during the normal stress or pore pressure oscillations, indicated by dashed blue line.

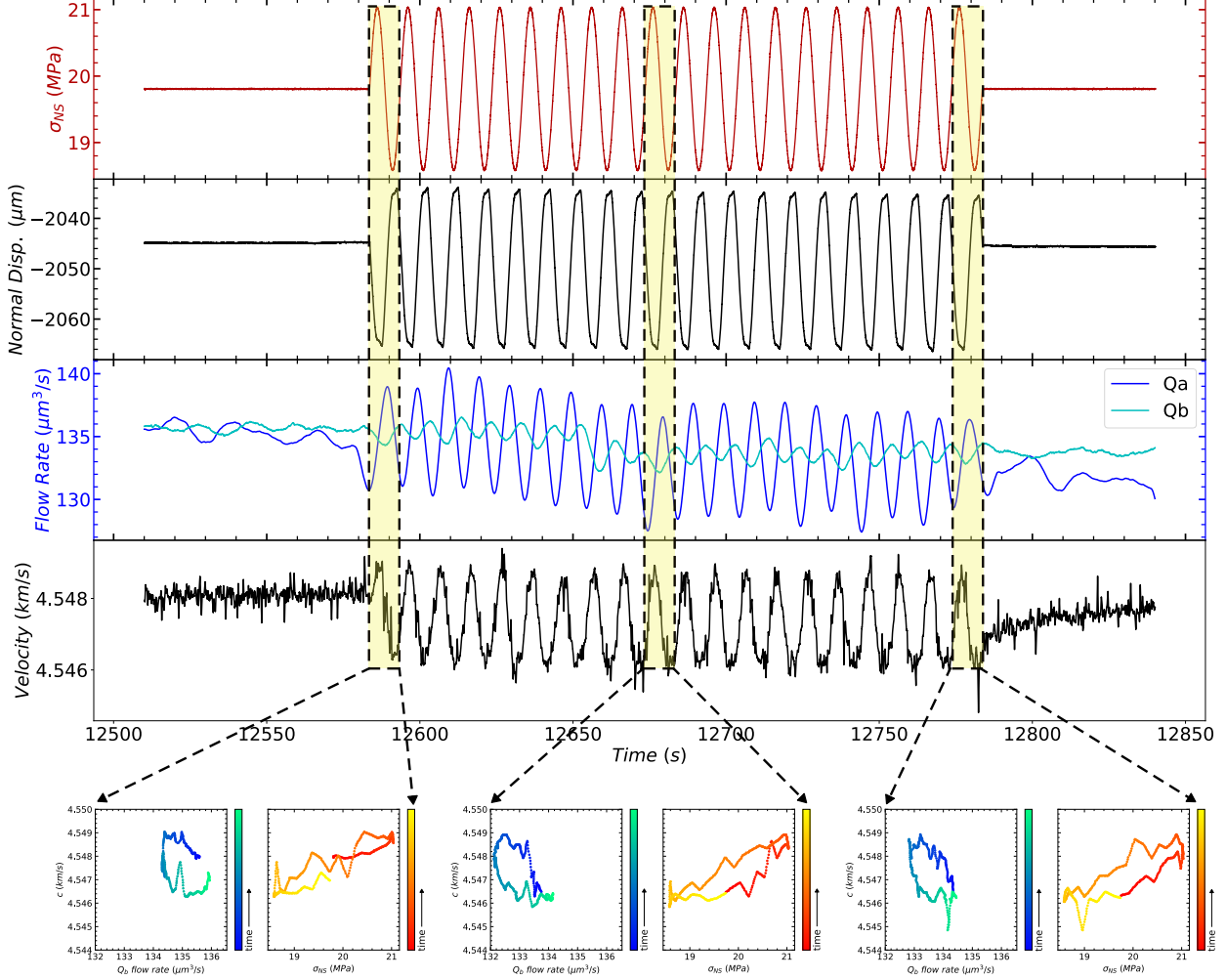


Figure 7: (a) Direct response of normal displacement, flow rate (inlet and outlet), and ultrasonic velocity for the direct path pair during a 0.1Hz 1MPa Normal Stress oscillation. Note the phase delay between the inlet and outlet flow rates. (b) shows how velocity varies as a function of outlet flow rate, Q_b , during the last cycle of the normal stress oscillation. The velocity increases with decreasing flow rate during compression and then the opposite trend with tension. The point to make here is that the fracture is continuously changing – the change in aperture results in change in velocity and flow paths. (c) Ultrasonic velocity as a function of the last full cycle of the normal stress oscillation.

Delineate (b) & (c) to distinguish compression and tension of oscillation.

6.2 perm evolution

perm evolution: transient response to dynamic stressing & shear: The stress-induced changes in permeability are captured by two parameters: (1) The transient change in permeability $\Delta k/k_0$ defined as the %-change due to the imposed normal stress or pore pressure oscillations, normalized by the pre-oscillation permeability k_0 as illustrated in Figure 2c (Candela et al., 2014) and (2) The recovery rate of permeability after the transient increase k_r .

Oscillation Amplitude- and Frequency-Dependencies: The dependencies of $\Delta k/k_0$ on the amplitude (Figure 5) and frequency of normal stress and pore pressure oscillations are given in Shokouhi et al. (2019). One important observation is that although small-amplitude oscillations ($< 0.5\text{ MPa}$) may result in a decrease in permeability, large-amplitude oscillations generally increase permeability transiently. Furthermore, for the same oscillation amplitude and frequency, the pore pressure oscillations appear to be more effective in permeability enhancement ($\Delta k/k_0 > 0$) than the normal stress oscillations by a factor of 2.5, particularly for sample WG1. In addition, $\Delta k/k_0$ increases, albeit slightly, with the frequency of oscillations (not shown here). The only exception is the decrease in $\Delta k/k_0$ for sample WG2, when we increase the fluid pressure oscillations from 1 Hz to 10 Hz. The details on amplitude- and frequency-dependencies of $\Delta k/k_0$ are given in Shokouhi et al. (2019). The recovery rate k_r does not show clear amplitude- and frequency-dependencies (not shown here).

Influence of Shearing: Generally speaking, after shearing the fracture, the normal stress oscillations become less effective in enhancing the fracture permeability (see Figure 5a). The trend is less obvious for pore water pressure oscillations (see Figure 5b).

correspondence b/w stiffness & perm transients: The main hypothesis driving this study was that the transient elastic softening is associated with a temporary increase in porosity and/or permeability, both of which are important for energy production and waste storage. Our results to date support this conjecture: the relative changes in wave velocity and permeability of fresh fractures (before shearing), due to both normal stress and pore pressure oscillations, are correlated, such that a larger drop in wave velocity (more negative $\Delta c/c_0$, equivalent to larger transient softening or higher nonlinearity) corresponds to a larger permeability enhancement $\Delta k/k_0$. As shown in Figures 6a and 6b (left panels), this overall correlation seems to hold for both normal stress and pore pressure oscillations. Furthermore, the recovery rates of wave velocity and permeability transients (c_r and k_r) also seem to be correlated (Figure 7), although there is slightly more scatter. This observation further reinforces the presumed linkage between the evolution of fracture's elastodynamic and flow properties. In other words, the form of the measured permeability transients is similar to that for the nonlinear elastic effects and both recoveries follow the time-logarithmic trajectories observed in the field or in nature. We should note that the correlations shown in Figure 6 correspond to $\Delta c/c_0$ averaged for 5 transducer pairs shown in Figure 1d. Examining the results for individual transducer pairs (not shown here) reveals the strong dependency of the measurements on the wave path. This is not surprising as the fracture aperture is nonuniform and the ray paths sample different portions of that interface.

Shearing the fracture appears to alter these relations indicating the influence of contact stiffness and shear fabric on both sets of properties (Figure 6a and 6b). Overall, shearing seems to weaken the correlation between $\Delta c/c_0$ and $\Delta k/k_0$ (Figure 6a and 6b, middle and right panels). The question remains as to what underlying micro-mechanisms link the nonlinear elastodynamic behavior and hydraulic properties of fractures.

We considered two mechanisms for this observed correspondence: (1) the unclogging of fracture flow conduits via fluid pressure oscillations, and (2) the dependence of both properties on stress-induced changes in the fracture aperture. Previous work shows that particle clogging can alter permeability via dynamic stressing in Berea sandstone (Elkhouri et al., 2011; Candela et al., 2014, 2015). However, for fractures in Westerly Granite we observe an increase in permeability for both pore pressure and normal stress oscillations of sufficiently large amplitude. With the new insights from the coupled ultrasonic data, one may conclude that unclogging is merely one of many potential mechanisms.

The other explanation for the linkage between stiffness and flow properties of fractured rocks could be the dependence of both properties on the fracture aperture change due to the imposed stress oscillations.

To further examine this hypothesis, we investigated whether delc/c_0 or delk/k_0 correlate with the measured changes in sample thickness changes (proxy for aperture compaction/dilation) during imposed oscillations (Shokouhi et al., 2019). However, we did not observe a strong correlation. This lack of strong correlation suggests that changes in fracture aperture cannot be the sole driving mechanism for permeability change, especially when driven by pore pressure oscillations.

We also used high-resolution optical profilometry to measure the roughness across the post-mortem fractured surfaces in order to reconstruct the fracture aperture distribution. However, since the fractures were created in-situ and were sheared twice before the roughness measurements, we do not have information on the aperture or roughness of fracture interfaces immediately post-fracture nor immediately post-shear (1st shearing step).

From Prabaha's Arma: The nonlinear parameter $\text{delc}/\text{c}0$ is plotted against the applied normal stress oscillation amplitude (0.2-1MPa) in Figure 5. The sample is more nonlinear if the absolute value of $\text{delc}/\text{c}0$ is larger at a given oscillation amplitude and frequency. As shown in Figure 5 (a) $\text{delc}/\text{c}0$ of the intact sample increases as the normal stress amplitude increases. Also, the nonlinearity seems to increase with the oscillation frequency. This trend closely resembles previous observations in dry intact Berea sandstone (Riviere et al., 2016). Similar trends are observed for the fractured sample in dry (Figure 5 (b)) and saturated (Figure 5 (c)) states. The results for the saturated fractured sample at 1Hz are also comparable to our previous observations on in-situ-stressed fractured samples of Westerly granite (Shokouhi et al., 2019).

We observe that the saturated fractured sample exhibits less nonlinearity than both the dry intact and fractured samples. For an intact sample, saturation decreases the pore compressibility, which increases wave velocity (Winkler and McGowan, 2004) and decreases nonlinearity (Ostrovsky and Johnson, 2001; Van Den Abeele, 2002). A decrease in the nonlinearity of an intact saturated rock sample has also been reported by Van den Abeele et al, 2002, Johnson et al., 2004 using a resonance-based method. For the saturated fractured sample, the decrease in the measured nonlinearity is due to the presence of the fluid and the resulting increased interface stiffness (Dwyer-Joyce, Zhu and Reddyhoff, 2010; Ooi and Dwyer-Joyce, 2016).

Figure 7 shows the normal stress amplitude- and frequency-dependency of the second extracted nonlinearity parameter $\text{dc}/\text{c}0$ for the sample in the three states. Similar to $\text{delc}/\text{c}0$, $\text{dc}/\text{c}0$ scales linearly with amplitude although, the trend here is clearer. A linear dependency is also apparent in dry intact Berea sandstone (Riviere et al., 2015). In addition, there is no discernible dependency on the frequency of oscillations. This observation aligns with that reported in a previous study (Riviere et al., 2016), where $\text{dc}/\text{c}0$ or the second harmonic amplitude was observed to be independent of the imposed oscillation frequency. Similar to what was observed for $\text{delc}/\text{c}0$, the dry intact sample appears more nonlinear than the dry fractured sample, which exhibits more nonlinearity than the saturated fractured sample.

6.3 Nonlinear Elastodynamic Response: Relative Change in Velocity and Permeability

- nonlinearity modulated by oscillation amplitudes
 - nonlinearity and permeability enhancement generally increase with frequency of dynamic stressing.
 - relative changes in wave velocity and permeability are correlated: larger drops in velocity — \downarrow larger increases in permeability
 - changes in permeability are greater at higher oscillation amplitudes
- Perm enhancement pronounced for Pp oscillations than for NS.

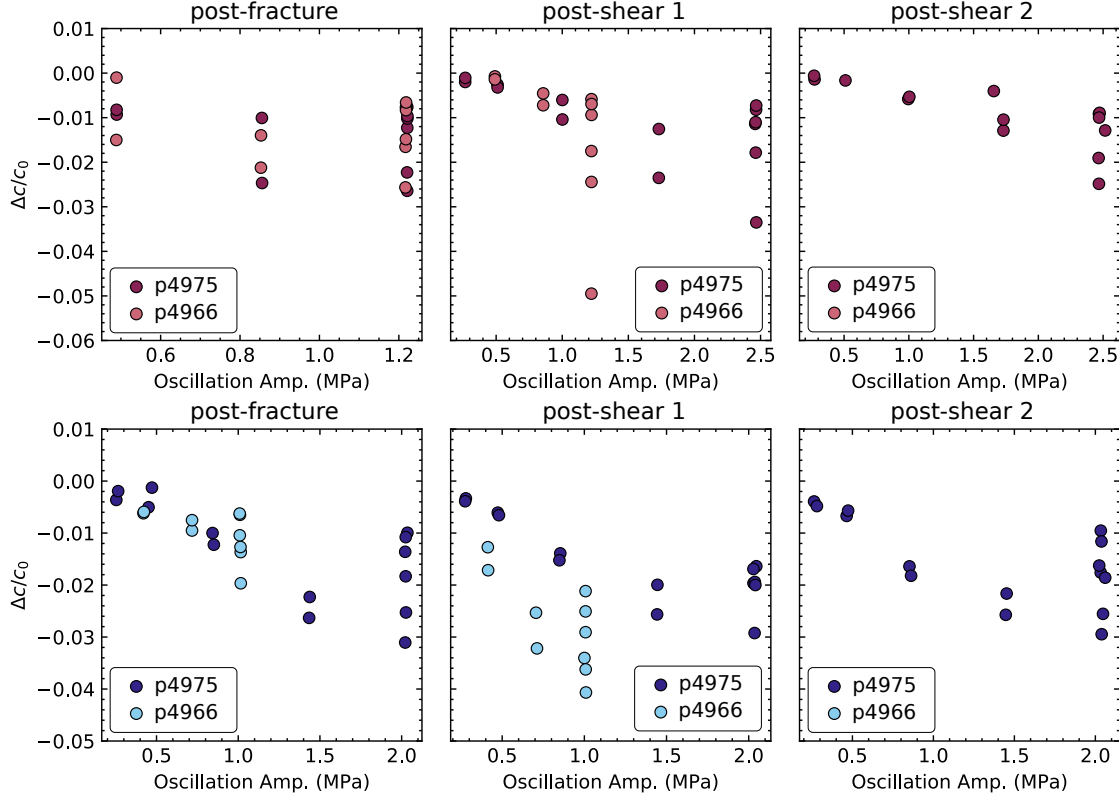


Figure 8: Nonlinearity as a function of σ_{NS} oscillation amplitude. Transitioning from post-fracture results to post-shear results, we observe decreased nonlinearity and permeability enhancement. This is probably related to clogging mechanisms.

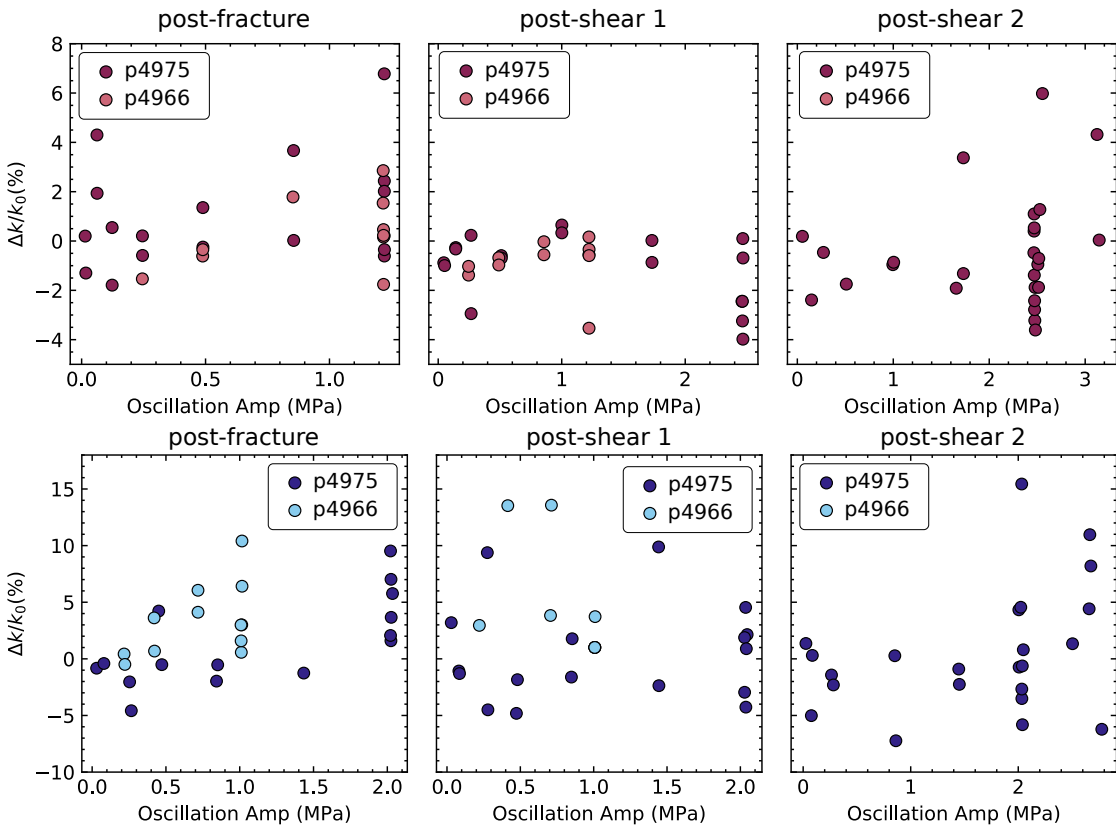


Figure 9: Change in permeability as a function of σ_{NS} oscillation amplitude. Transitioning from post-fracture results to post-shear results, we observe decreased nonlinearity and permeability enhancement. This is probably related to clogging mechanisms.

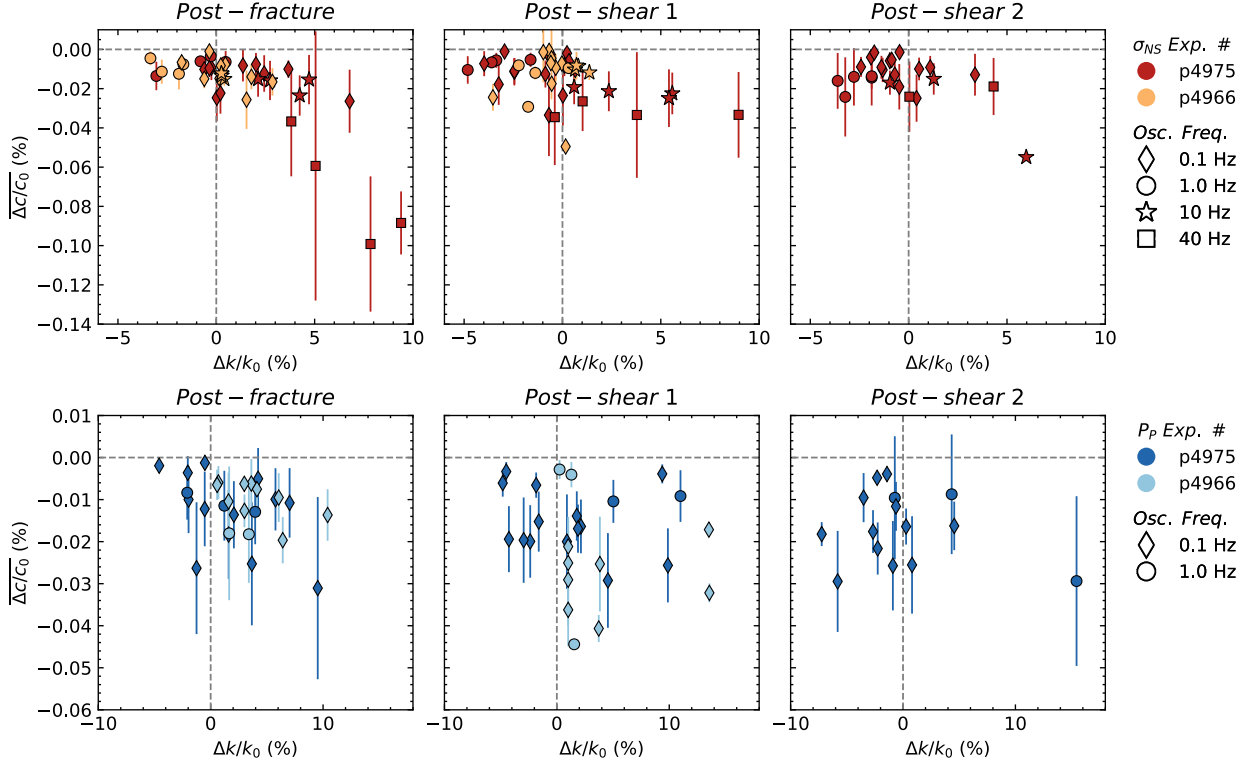


Figure 10: Nonlinearity as a function of permeability change for σ_{NS} and P_p oscillations averaged over all receivers. Permeability is an averaged measurement across the fracture, so these parameters should exhibit some relationship. I don't know what this says about the mechanisms at play. Maybe the contact area has been reduced (lower nonlin) and also maybe wear material was mobilized during P_p oscillation and temporarily increased contact area (higher nonlin). Does this match with reality – does shearing the fracture increase the contact area? My intuition agrees with this, but it is conceivable that with a complex geometry, this could be more complex.

6.4 Velocity Amplitude Modulation during Perturbations

- Although the origins of dc/c_0 and dc/c remain unclear, consider empirical evidence from [Rivière et al., 2015, 2016] that they originate from different micro-scale mechanisms

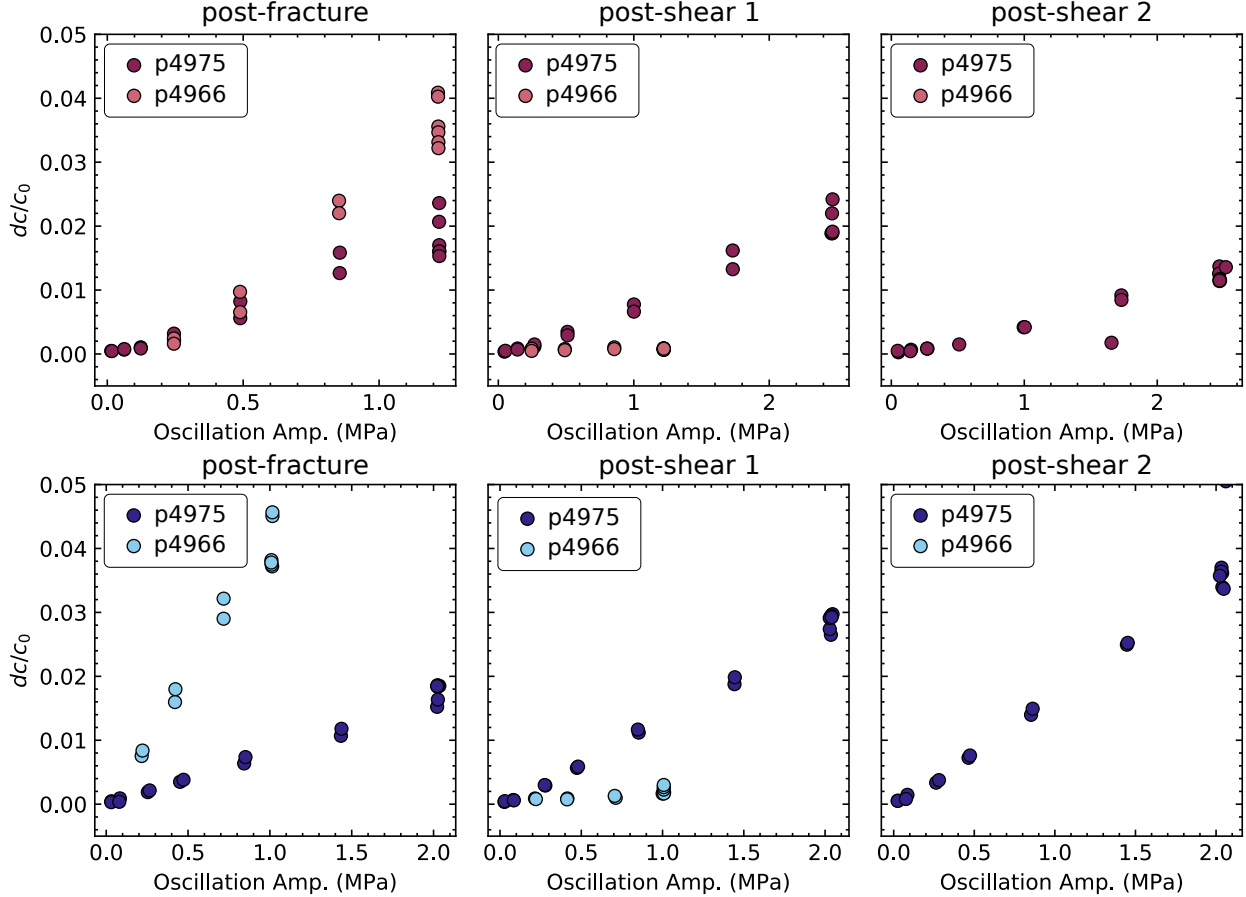


Figure 11: Velocity amplitude modulation averaged over all receivers (dc/c_0) as a function of permeability recovery (k) for NS and PP oscillations. I suspect that we are not waiting long enough to see a trend like J. Elkhouri and others. His recovery values were 0.5, which he says is related to the dimensionality of the fracture. Shearing the fracture increases the complexity and maybe changes the slope – dominated by clogging/moving wear material rather than mated aperture.

6.5 Recovery of Velocity and Permeability

- Although the origins of $\Delta c/c_0$ and dc/c remain unclear, consider empirical evidence from [Rivière et al., 2015, 2016] that they originate from different micro-scale mechanisms

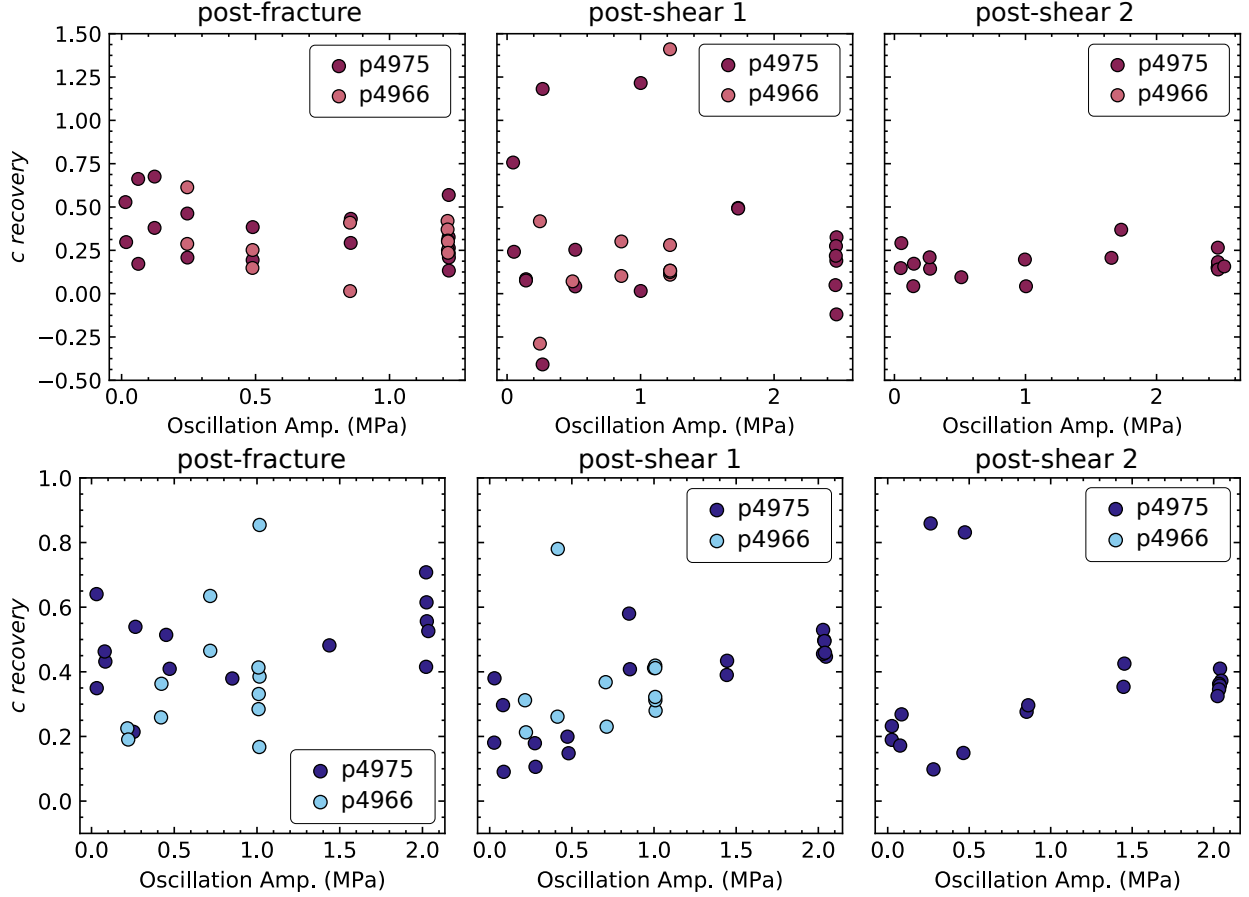


Figure 12: Velocity recovery averaged over all receivers (\bar{c}) as a function of oscillation amplitude for NS and PP oscillations. I suspect that we are not waiting long enough to see a trend like J. Elkhouri and others. His recovery values were 0.5, which he says is related to the dimensionality of the fracture. Shearing the fracture increases the complexity and maybe changes the slope – dominated by clogging/moving wear material rather than mated aperture.

6.6 Effect of Fracture Aperture

- effect of fracture aperture modulated by shearing the fractured samples in two 5mm increments, repeating the dynamic stressing protocols. Elucidates how changes in the aperture size distribution due to shearing and wear alter the fracture stiffness and the stress-dependency.
- shearing of the fracture reduces the nonlinearity measured during normal stress oscillations
- oscillations become generally less effective in enhancing the fracture permeability.
- the correlation between the nonlinearity and permeability change and sample thickness change is stronger for NS oscillations than Pp.
- There is no clear correlation between perm change and flow rate during oscillations, suggesting “unclogging” may not be the sole mechanism responsible for perm change due to Pp oscillations.
- However, we report nonlinearity after the second shear history: indicative of possible differences in mechanisms activated during the two modes of stressing.

7 Supplemental

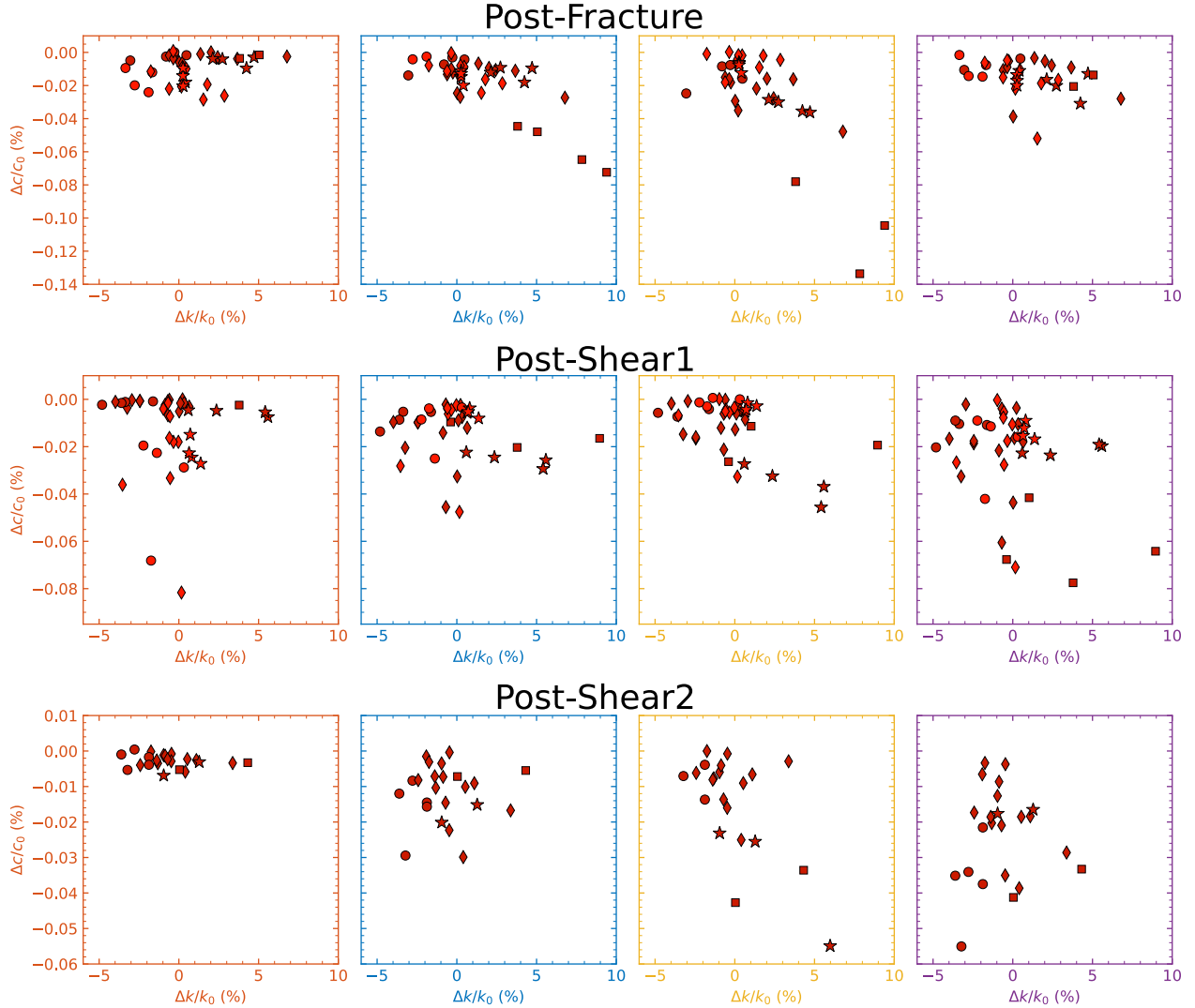


Figure 13: Nonlinearity as a function of permeability change for σ_{NS} oscillations for each receiver. Transitioning from post-fracture results to post-shear results, we observe decreased nonlinearity and permeability enhancement. This is probably related to clogging mechanisms.

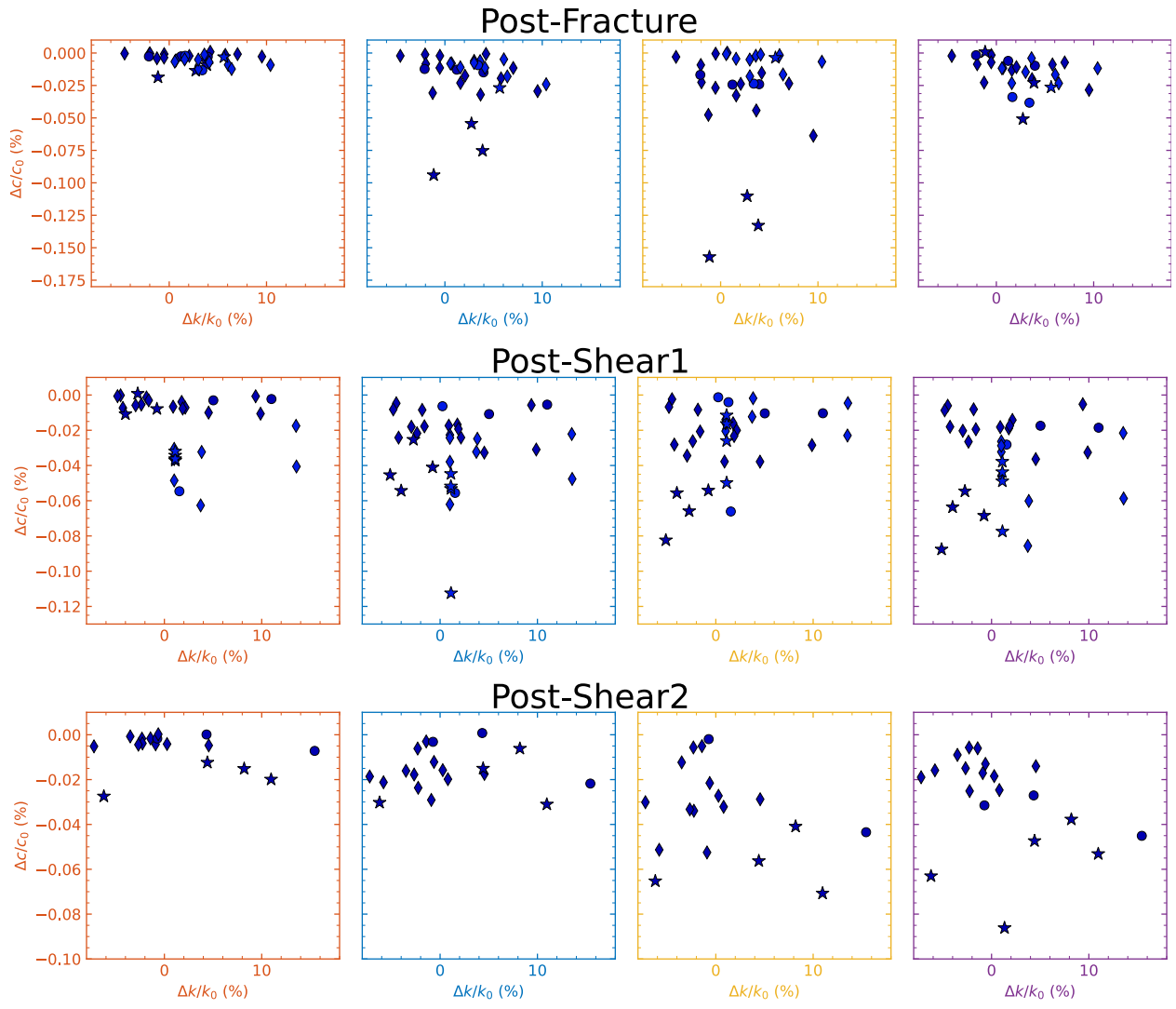


Figure 14: Nonlinearity as a function of permeability change for P_P oscillations for each receiver.